Hydrogen Atom Loss from the Benzene Cation. Why Is the Kinetic Energy Release so Large?†

E. Gridelet, A. J. Lorquet, R. Locht, J. C. Lorquet, and B. Leyh*

Department of Chemistry, Molecular Dynamics Laboratory, Building B6c,University of Liège, B-4000 SART-TILMAN, Belgium

Received: October 25, 2005; In Final Form: December 22, 2005

The kinetic energy release distributions (KERDs) associated with the hydrogen loss from the benzene cation and the deuterium loss from the perdeuteriobenzene cation have been remeasured on the metastable time scale and analyzed by the maximum entropy method. The experimental kinetic energy releases are larger than expected statistically, in contradistinction to what has been observed for the C−X fragmentations of the halogenobenzene cations. H(D) loss from $C_6H_6^+$ ($C_6D_6^+$) occurs via a conical intersection connecting the $^2A_2$ and $^2A_1$ electronic states. Two models are proposed to account for the experimental data: (i) a modified orbiting transition state theory (OTST) approach incorporating electronic nonadiabaticity; (ii) an electronically nonadiabatic version of the statistical adiabatic channel model (SACM) of Quack and Troe. The latter approach is found to be preferable. It leads to the conclusion that the larger the energy stored in the transitional modes, which partly convert to the relative interfragment motion, the shorter the value of the reaction coordinate at which the adiabatic channels cross, and the larger the probability of undergoing the $^2A_2 \rightarrow {}^2A_1$ transition required for hydrogen loss.

I. Introduction

The unimolecular dissociation of the benzene ion into a phenyl ion and a hydrogen atom has always been somewhat of a mystery. The reaction presents no reverse activation barrier and hence no obvious transition state. Its rate constant and those of competitive pathways have received extensive attention[1−19] and RRKM calculations with a tight transition state have been found to account for the experimental H-loss data.[11−13] Klippenstein used variational transition state theory (VTST) to model the reaction[16] and determined the electronic energy curves as a function of the hydrogen−carbon distance.[20]

However, the distribution of the released translational kinetic energy (KERD) has also been measured.[7,8,21−25] Jarrold et al.[8] concluded that a transition state switching model was able to account for the rate constant but not for the KERD. Klots[21] used his version of phase space theory and reached a similar conclusion.

Lifshitz[26] generalized the problem and noticed that translational energy releases for H atom losses are usually much greater than expected from phase space theory.[8,21,27−30]

It has been found by us in a previous study[31] that for reactions leading to the loss of a hydrogen atom, the orbiting transition state theory (OTST)[28,31−37] loses any validity, at least at energies representative of mass spectrometric experimentation with sector instruments. The reason for this failure can be traced back to the breakdown of two essential assumptions of OTST: (i) the ion-induced dipole approximation postulated in the Langevin model is not valid at the transition state and (ii) the angular and radial degrees of freedom can no longer be adiabatically separated as the reaction is not rotationally adiabatic. Therefore, no quantitative study based on phase space theory is possible for hydrogen-loss reactions.

The present contribution does not focus on the rate constant, but on the KERD for the H-loss from the benzene cation,

$$C_6H_6^+[(\sigma_{CH})^2\pi^5]\ (^2B_1 \text{ or } {}^2A_2) \rightarrow C_6H_5^+[\pi^6]\ (^1A_1) + H[1s_H]\ (^2S) \quad (1.1a)$$

and for the equivalent reaction for the perdeuterated species,

$$C_6D_6^+ \rightarrow C_6D_5^+ + D \quad (1.1b)$$

One of the essential characteristics of this fragmentation is its inherently electronic nonadiabatic nature due to the difference in the electronic configurations of the reactant and of the product ground states, as established by Klippenstein[20] and later confirmed by independent ab initio calculations.[38] A positive hole is located in the π shell of the benzene ion in its ground state, whereas the π shell of the phenyl cation is fully occupied in the ground state.[20,38,39] Such a situation necessarily leads to a conical intersection between the two potential energy surfaces. By a joint experimental and theoretical study, the present work aims at relating the observed characteristics of the KERD to the peculiar properties of the reaction, especially its electronic nonadiabaticity.

An interesting element of appreciation results from a comparative study of the KERD measured for various reactions

$$C_6H_5X^+ \rightarrow C_6H_5^+ + X \quad (1.2)$$

The maximum entropy method[40−42] analyzes KERDs by comparing them with a purely statistical distribution computed from the density of states of the dissociation fragments. Therefore, the same statistical distribution corresponds to all fragmentations into a phenyl ion and an atom X. However, these dissociations proceed in an entirely different way depending on whether X is a hydrogen or a halogen atom. When X = I or Br, the reaction

† Part of the "Chava Lifshitz Memorial Issue".

* Corresponding author. E-mail: Bernard.Leyh@ulg.ac.be. Telephone: ++32-4-3663425. Fax: ++32-4-3663413.

10.1021/jp056119h CCC: $33.50
Published on Web 02/15/2006

mechanism is known to be electronically adiabatic. Furthermore, the average translational energy release $\langle\epsilon\rangle$ is less than the estimate $\langle\epsilon\rangle^0$ derived from a purely statistical theory.[43,44] Finally, it has been shown in a recent study that at low total energies, OTST is valid when X is a halogen.[31] We shall show in this paper that the characteristics of reaction 1.2 when X = H are radically different with respect to the following features: (i) the reaction is electronically nonadiabatic, (ii) OTST is invalid, and (iii) the actual average translational energy release $\langle\epsilon\rangle$ is larger than the statistical estimate $\langle\epsilon\rangle^0$.

The paper is organized as follows. The experimental technique and the maximum entropy method are summarized in sections II and III, respectively. The results are presented in section IV. Section V deals with quantum ab initio calculations concerning the electronic nonadiabaticity of the title reaction. An attempt to incorporate the nonadiabatic mechanism in OTST is discussed in section VI. Section VII analyzes in detail the consequences of electronic nonadiabaticity in the framework of the statistical adiabatic channel formalism (SACM).[45−47] Concluding remarks are formulated in section VIII.

II. Experiment

The experimental setup used to measure kinetic energy release distributions is a forward geometry (EB) sector mass spectrometer. The spectrometer includes the following: (i) an ion source where benzene molecules are ionized by electron impact and accelerated to keV translational energies; (ii) a first field free region; (iii) an electrostatic sector; (iv) a second field free region; (v) a magnetic sector; (vi) an ion detector.

The accelerating voltage scan technique makes possible to record the parent ion spectrum of all metastable dissociations leading to a selected fragment ion in the first field-free region.[48−50] The release of translational energy upon fragmentation broadens the recorded peaks. As instrumental broadening also takes place, a preliminary deconvolution step is required.[30] Then, a kinetic energy release distribution can be deduced from the deconvoluted peak by a differentiation procedure and a change of variables from the laboratory to the center-of-mass reference frame.[51−53] Angular discrimination effects are negligible in the present case, so that more elaborated data treatments[54−56] are not required.

Benzene (commercially available from Merck with 99.9% purity for C_6H_6, and from Aldrich with 98% purity for C_6D_6) was used without further purification. In the spectrometer source, the kinetic energy of the ionizing electrons is equal to 70 eV and the emission current is set at 10 μA. The electrostatic analyzer exit slit (β-slit) is closed to 0.25 mm to reach an energy resolution $\Delta E/E$ of 10^{-3}.

In this setup, dissociations are sampled in a given time window defined by the entrance time (τ_1) into, and the exit time (τ_2) out of the first field free region. Accordingly, the total energy distribution of the parent ions is given by the following transmission function $T(E)$

$$T(E) = N\,[\exp(-k(E)\tau_1) - \exp(-k(E)\tau_2)]R(E) \quad (2.1)$$

where N is a normalization factor, $k(E)$ is the dissociation rate constant, whose variation with internal energy is available for $C_6H_6^+$[3,4,7,9,11,12,14−17] and $C_6D_6^+$.[12,14,15] $R(E)$ is the branching ratio for the hydrogen loss channel.[11] To sample different internal energy ranges, three translational energies of the ionic fragment (2, 5, and 8 keV in the laboratory frame) were selected. Average internal energies (measured from the lowest H(D)-loss asymptote) are summarized in Table 1. The energy ranges sampled by both isotopomers are clearly different. The thermochemical dissociation threshold measured with respect to the ground state of the neutral molecule has been taken equal to 13.03 eV for reaction 1.1a[57] and to 12.98 eV for reaction 1.1b.[12]

TABLE 1: Average Kinetic Energy Release $\langle\epsilon\rangle$ and Ergodicity Index F at the Average Energy $\langle E\rangle$[a]

	translational energy (keV)	$\langle E\rangle$ [eV]	$\langle\epsilon\rangle(\langle E\rangle)$ [eV]	F($\langle E\rangle$) [%]
$C_6H_5^+ + H$	2	1.21	0.177 ± 0.005	91 ± 2
$C_6H_5^+ + H$	5	1.27	0.194 ± 0.005	87 ± 2
$C_6H_5^+ + H$	8	1.30	0.224 ± 0.007	76 ± 3
$C_6D_5^+ + D$	2	1.58	0.179 ± 0.004	96 ± 1
$C_6D_5^+ + D$	5	1.64	0.200 ± 0.005	91 ± 1
$C_6D_5^+ + D$	8	1.68	0.209 ± 0.004	90 ± 1

[a] The second column indicates the fragment ion translational energy in the laboratory reference frame.

III. Maximum Entropy Method

Let us denote by $P(\epsilon|E)$ the probability of releasing a relative kinetic energy ϵ on the dissociation fragments when the system total energy is equal to E. Since the considered system is the pair of fragments, E is measured in this paper, unless otherwise stated, with respect to the lowest $C_6H_5^+ + H$ or $C_6D_5^+ + D$ dissociation asymptote.

The maximum entropy method compares an experimental distribution, here $P(\epsilon|E)$, with the corresponding full statistical distribution, called the prior distribution. In the field of unimolecular dissociations, the statistical situation arises when the ergodicity assumption of statistical theories is fulfilled: all product quantum states are equally probable. Therefore, the prior distribution $P^0(\epsilon|E)$ is proportional to the density of states corresponding to a translational energy ϵ at a total energy E[35,40−42,58,59]

$$P^0(\epsilon|E) = N^0(E)\epsilon^{1/2}\int_0^{E-\epsilon} \rho_{rot}(E_{rot})\,\rho_{vib}(E - \epsilon - E_{rot})\,dE_{rot} \quad (3.1)$$

where $N^0(E)$ is a normalization factor, ρ_{vib} is the vibrational density of states of the fragments, ρ_{rot} is their rotational density of states, and where the density of translational states for a three-dimensional motion is proportional to $\epsilon^{1/2}$.

If a dynamical constraint $A(\epsilon)$ prevents phase space from being fully explored, $P(\epsilon|E)$ will be different from $P^0(\epsilon|E)$. The distribution that accounts for this constraint but is otherwise of maximum entropy can be related to $P^0(\epsilon|E)$ by the following equation[40−42]

$$P(\epsilon|E) = P^0(\epsilon|E)\exp[-\lambda_0(E) - \lambda(E)\,A(\epsilon)] \quad (3.2)$$

where λ_0 ensures normalization and λ is the Lagrange multiplier conjugated to the constraint. In the general formalism, a sum of terms $\sum_i \lambda_i A_i(\epsilon)$ is used in eq 3.2,[41,60] but in many instances, the introduction of a single constraint has been found to be sufficient.[43,44,61−64]

The distribution $\tilde{P}(\epsilon)$ that can be compared to the experimental data is an average of $P(\epsilon|E)$ over the total energy distribution $T(E)$

$$\tilde{P}(\epsilon) = \int_\epsilon^\infty P^0(\epsilon|E)\exp[-\lambda_0(E) - \lambda(E)\,A(\epsilon)]\,T(E)\,dE \quad (3.3)$$

Similarly, $\tilde{P}^0(\epsilon)$ is defined as the average of $P^0(\epsilon|E)$ over $T(E)$. Equation 3.3 is then fitted to the experimental distribution in order to obtain $\lambda(E)$ and $A(\epsilon)$.

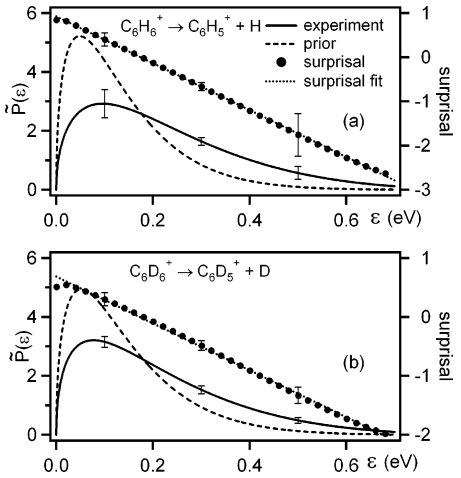

Figure 1. Left axis, solid line: experimental KERD for $C_6H_6^+ \rightarrow C_6H_5^+ + H$ (a) and $C_6D_6^+ \rightarrow C_6D_5^+ + D$ (b) for a fragment ion translational energy equal to 8 keV in the laboratory reference frame. Dashed line: prior KERD, $\tilde{P}^0(\epsilon)$, computed for the same total energy distribution $T(E)$. Right axis, full circles: surprisal $\tilde{I}(\epsilon)$. Dotted line: surprisal fit. Typical error bars are provided. Large uncertainties in the surprisal at large ϵ result from the division by small values of $\tilde{P}(\epsilon)$ (see eq 3.4).

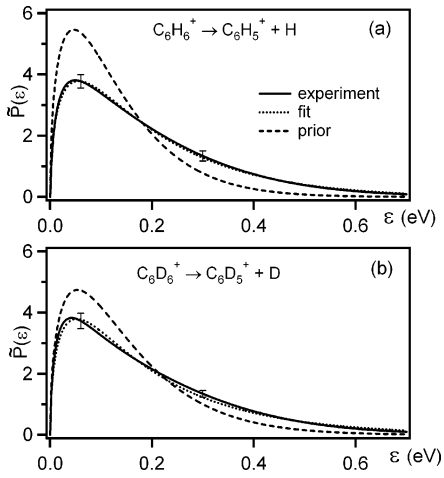

Figure 2. Solid line: experimental KERD for $C_6H_6^+ \rightarrow C_6H_5^+ + H$ (a) and $C_6D_6^+ \rightarrow C_6D_5^+ + D$ (b) for a fragment ion translational energy equal to 2 keV in the laboratory reference frame. Dashed line: prior KERDs $\tilde{P}^0(\epsilon)$ computed for the same total energy distributions $T(E)$. Dotted line: fit to the experimental KERD using eq 3.3 with $A(\epsilon) = \epsilon$. Typical error bars are given at only two kinetic energies in order not to overcrowd the figure.

A visual way to estimate $A(\epsilon)$, if λ_0 and λ are assumed to be independent of E, is to compute the average surprisal, $\tilde{I}(\epsilon)$, resulting from the discrepancies between the experimental and the prior distribution

$$\tilde{I}(\epsilon) = \ln[\tilde{P}^0(\epsilon)/\tilde{P}(\epsilon)] \approx \lambda_0 + \lambda A(\epsilon) \qquad (3.4)$$

and to find the functional form of $A(\epsilon)$ that linearizes the surprisal $\tilde{I}(\epsilon)$.[61]

The entropy S of a distribution is directly linked to the number of configurations that give rise to this distribution. Hence, the prior distribution, i.e., the most statistical distribution, corresponds to the maximum possible entropy $S°$. The entropy deficiency $DS = S° - S$ that represents the difference between the prior and the actual entropies is

$$DS(E) = \int_0^E P(\epsilon|E) \ln [P(\epsilon|E)/P^0(\epsilon|E)]\, d\epsilon = -\lambda_0(E) - \lambda(E)\, \langle A(\epsilon)\rangle \qquad (3.5)$$

The entropy deficiency leads to another essential parameter: the ergodicity index

$$F(E) = \exp[-DS(E)] \qquad (3.6)$$

which is an upper bound for the ratio between (i) the phase space volume effectively explored during the reaction and (ii) the phase space volume available for the system at the energy E.[41,65] This parameter thus measures to what extent the reaction is ergodic.

IV. Results

A. Kinetic Energy Release Distributions and Surprisal Fits. Experimental KERDs are displayed in Figure 1 with the corresponding prior distributions. We tried to linearize the surprisal $\tilde{I}(\epsilon)$ using various powers of ϵ and found that the best fit simply occurs for $A(\epsilon) = \epsilon$ as shown in the figure. This is in contrast with nearly all previous studies,[30,43,44,61,62] which had observed a constraint equal to $\epsilon^{1/2}$.

Fitting the experimental data using either a constant λ or a linear variation of λ as a function of E leads to nearly identical results at the average internal energy, $\langle E\rangle$, as already observed in the analysis of the pyridine dissociation.[63] The fitted value of λ at this energy is therefore especially robust and will be used thereafter to calculate the average kinetic energy $\langle\epsilon\rangle$ and the ergodicity index F. Three values of λ have been deduced, corresponding to the three $\langle E\rangle$ values associated with experiments at, respectively, 2, 5, and 8 keV (see section II and Table 1). In an alternative data treatment procedure, the KERDs corresponding to these three energy ranges have been fitted using a single parametric linear function $\lambda(E)$, by minimizing the sum of their respective chi-squared, χ^2. $\lambda(E)$ is found to be negative and decreasing upon increasing E. As an example, the experimental (2 keV) and fitted data are compared in Figure 2.

B. Average Kinetic Energy and Ergodicity Index. Once $\lambda(E)$ has been obtained, the average translational energy release at a given energy E can be calculated from the maximum entropy equation:

$$\langle\epsilon\rangle(E) = \int_0^E \epsilon P^0(\epsilon|E) \exp[-\lambda_0(E) - \lambda(E)A(\epsilon)]\, d\epsilon \qquad (4.1)$$

The resulting curve is drawn in Figure 3. In addition, for each individual measurement at a given acceleration voltage, the value of $\langle\epsilon\rangle$ is particularly reliable at $E = \langle E\rangle$. Figure 3 and Table 1 provide these data. Also represented is the statistical expectation $\langle\epsilon\rangle^0$, calculated as the first moment of the prior distribution $P^0(\epsilon|E)$. Clearly, resulting from the negative value of λ, the dynamics leads to a larger translational energy release than the statistical estimate when the released atom is either H or D. The reverse situation is observed when X is a halogen atom.[43,44]

These points $\langle\epsilon\rangle(\langle E\rangle)$ are compatible with other metastable data available in the literature,[8,21−25,66] even though no precise information is provided concerning the energy domain reached in those experiments. The value found by Moon et al.,[66] and mentioned in Figure 3, corroborates the large increase of $\langle\epsilon\rangle$ with the total energy E.

An additional measurement has been performed on $C_6D_6^+$ by dissociative photoionization using the Ne(I) resonance line with a retarding potential device.[62−64,67,68] At $E = 1.6$ eV, $\langle\epsilon\rangle$ is found to be equal to 0.20 eV, a value comparable with the metastable data (Figure 3). Such measurements are, however,

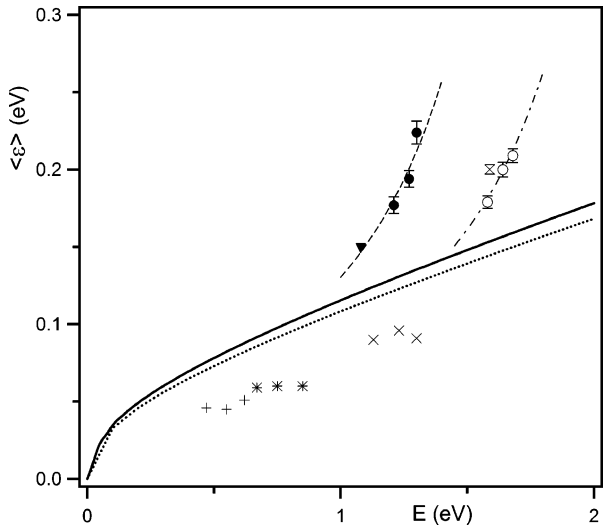

Figure 3. Average kinetic energy release $\langle\epsilon\rangle(E)$. Full circles: $C_6H_5^+ + H$ (this work, at $E = \langle E\rangle$ for each experimental set of data). Full triangle: $C_6H_5^+ + H$ (ref 66). Open circles: $C_6D_5^+ + D$ (this work, at $E = \langle E\rangle$ for each experimental set of data). Open hourglass: $C_6D_5^+ + D$ (this work, at $E = \langle E\rangle$ for the dissociative photoionization experiment with Ne(I)). Crosses: $C_6H_5^+ + X$ (X = Cl, Br, I) (ref 43 and 44). The dashed (reaction 1.1.a) and dash−dotted (reaction 1.1.b) lines correspond to a fit with a common $\lambda(E)$ for the three internal energy ranges, with $A(\epsilon) = \epsilon$ (see text). The solid and dotted lines represent the first moment of the prior distribution, $\langle\epsilon\rangle^0(E)$, for the nondeuterated and for the perdeuterated species, respectively.

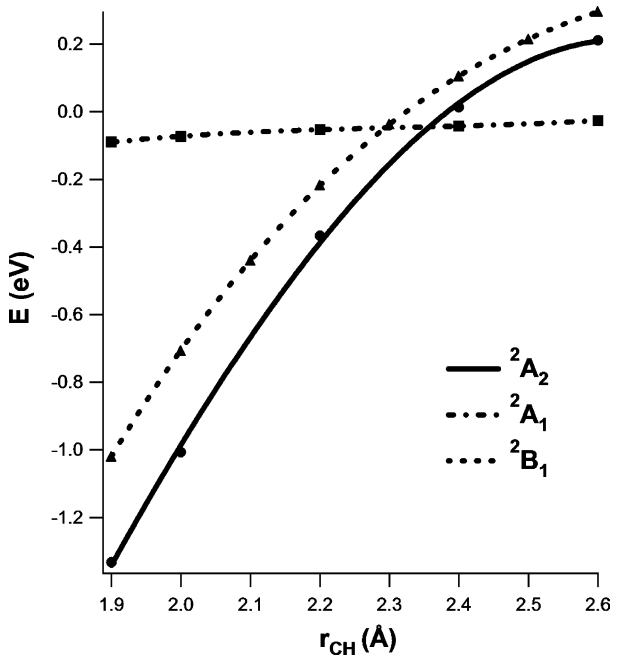

Figure 4. CASSCF(5,6)-6-31G(d) ab initio calculations of the potential energy curves of $C_6H_6^+$ along the C−H coordinate (C_{2v} point group) for the $^2A_2$, $^2B_1$, and $^2A_1$ states in the region where nonadiabatic interactions take place. Geometry optimization for the remaining coordinates has been performed for each individual electronic state.

difficult because, in reaction 1.1b, the ionic fragment ($C_6D_5^+$) carries only 2% of the total kinetic energy release.

In Table 1, we see that energy flows quite efficiently between the reaction coordinate and the bath of internal oscillators: the ergodicity index, F (eq 3.6), is equal to 75−90% for $C_6H_6^+$ at $E \sim 1.25$ eV. It even reaches 90−95% for $C_6D_6^+$ ions which are sampled, in the metastable window, at higher energy ($E \sim 1.65$ eV). F is an upper bound because it is insensitive to any restriction on phase space sampling that does not affect the KERD (e.g., the flow of vibrational energy among oscillators).

V. Quantum Chemical Calculations: Electronic Nonadiabaticity

There is an extensive literature dealing with the electronic structure of the benzene cation. Most of it concerns the static and dynamic Jahn−Teller effects that take place in the neighborhood of the equilibrium geometry. However, the problem that has to be dealt with here concerns the nonadiabatic interaction that is encountered as one of the CH bonds is stretched and only the relevant portion of the reaction path has been studied. Complete active space self-consistent field [CASSCF(5, 6)] calculations were carried out with a 6-31G(d) basis set of atomic orbitals (102 basis functions). As a check, some portions of the potential energy surfaces were recalculated with the somewhat larger basis set 6-31G(d,p). The occupied and unoccupied spaces consisted each of one σ (a_1) and two π (b_1 and a_2) molecular orbitals. A total number of 210 configuration state functions were generated. Three low-lying electronic states ($^2A_2$, $^2A_1$, and $^2B_1$) have been studied. Note that Klippenstein[20] focuses on the $^2B_1$ and $^2A_1$ states. Geometry optimizations as a function of the reaction coordinate were carried out independently for each electronic state. The equilibrium geometry was found to belong to the C_{2v} point group in each case.

For moderate values of the reaction coordinate, the ground electronic state belongs to the $^2A_2$ representation. Its energy increases continuously as a function of the reaction coordinate. The aromatic cycle is nearly symmetrical in this state. The angle α at the dehydro carbon ranges between 120 and 123°. This ground state correlates diabatically with excited fragments, $C_6H_5^+$ ($^3A_2$) + H (^2S).

The next higher electronic state belongs to the $^2B_1$ representation. Its potential energy curve is nearly parallel to that of the $^2A_2$ state and is consistently located slightly above it. Its equilibrium geometry is characterized by a shortening of the two CC bonds that are parallel to the symmetry axis, with the angle α ranging between 124 and 125°.

At larger values of the reaction coordinate, the potential energy curves of these two states are crossed by that of a $^2A_1$ state, whose energy is nearly constant and which diabatically correlates with ground-state fragments, $C_6H_5^+$ ($^1A_1$) + H (^2S) (Figure 4). This type of crossing is termed a conical intersection. In the $^2A_1$ state, the cycle deforms and adopts a geometry similar to that of the phenyl ion fragment, with a particularly large value for the angle α, which now ranges between 142 and 147°. The $^2A_2$ and $^2A_1$ states were calculated to cross at a CH distance of 2.37 Å with the 6-31G(d) basis set and at 2.35 Å with the 6-31G-(d,p) basis set. This distance is compatible with Klippenstein's calculations that give a CH distance of 2.25 Å at the intersection between $^2B_1$ and $^2A_1$.[20]

Of prime interest in the dissociation mechanism is the conical intersection that connects the $^2A_2$ and $^2A_1$ states. The $^2B_1$ state plays no role in the dissociation dynamics of reaction 1.1. However, since its energy is close to that of the $^2A_2$ state, this quasi-degeneracy considerably complicates the ab initio calculations by creating instabilities and convergence difficulties.

When the CH distance is frozen at 2.37 Å, states $^2A_2$ and $^2A_1$ are found to be connected by a transition state that belongs to the C_2 point group (i.e., that presents a C_2 axis as its unique symmetry element). The height of the activation energy barrier is found to be equal to about 0.2 eV.

Switching from a $^2A_2$ to a $^2A_1$ state in the conical intersection requires no energy barrier. It involves in principle the participa-

tion of at least one antisymmetric bending mode apt to lower the symmetry in order to pass around the cone vertex. However, the distortion is thought to be insignificant here. Ab initio calculations carried out in the C_s point group led to distortion angles less than 1°, and the attempt was not pursued. Therefore, only calculations carried out in the C_{2v} point group are reported here.

Note finally that the ab initio results are of qualitative value only at large values of the reaction coordinate. An improvement of the situation would require a better introduction of the dynamic correlation energy through CAS-MP2 or CASSCF+MRCI calculations.

VI. Centrifugal Potential Barrier

The most surprising and interesting experimental result is that the benzene C−H fragmentation releases more kinetic energy than statistically expected, whereas the opposite is true for the halogenobenzene C−X fragmentations.

High translational energy releases are often rationalized by the presence of a reverse potential barrier.[30,35,36,64,69] However, our ab initio calculations, those of Nicolaides et al.,[38] and those of Klippenstein[20] agree about the absence of any reverse barrier of electronic origin. Furthermore, the main effect of an electronic barrier would be to shift the KERD along the kinetic energy axis from zero by an amount corresponding to part of its height.[30,36] This does not correspond to the experimental observations (Figures 1 and 2).

An alternative explanation involves a centrifugal barrier, as in OTST. Since the barrier height grows as the reduced mass of the fragments decreases, this proposal is a priori appealing for the loss of a hydrogen atom.

It will now be shown that, although OTST is not directly applicable for a H-loss reaction,[31] a discussion in terms of this theory provides useful qualitative insight into the reaction mechanism.

A modified OTST model had to be developed to account for the electronically nonadiabatic nature of the reaction. Instead of using a long-range charge-induced dipole potential, we have considered the two electronic energy curves for the $^2A_2$ and $^2A_1$ states (see section V), and have added to them the centrifugal potential $l(l+1)\hbar^2/2\mu r^2$, as illustrated in Figure 5. The $^2A_2$ state is described by a Morse potential, with parameters chosen to fit the ab initio data, and the $^2A_1$ potential is considered to be flat. Since the asymptote to which the $^2A_2$ state converges at about 1.3 eV [20] is not reached within our experimental energy range, the dissociating ion must switch from the $^2A_2$ state to the $^2A_1$ state around the crossing point, which now plays a role similar to that of the top of a barrier (see Figure 5). In this modified OTST model, the probability of observing a kinetic energy ϵ is related to the number of channels associated with a reverse barrier lower than ϵ. Moreover, each channel is weighted by the quantum probability, P, of crossing the nonadiabatic region along the adiabatic pathway at the kinetic energy ϵ. The available expression of P is especially appropriate to study weak nonadiabatic interactions involving tunneling.[70−73]

The resulting KERD is displayed in Figure 6, together with the prior and the experimental distributions.

The modified nonadiabatic OTST and prior distributions are observed to decrease much more steeply than the experimental one. Actually, this decrease is the result of the large number of $C_6H_5^+$ internal degrees of freedom, which pump nearly all the available energy. To illustrate this, let us assume that the density of vibrational states, $\rho_{vib}(E_{vib})$, is approximately proportional to $\exp(\omega E_{vib})$:[31] in the present case, $\omega \sim 10$ eV^{-1}. The prior and the modified OTST distributions are then proportional to $\exp(-\omega\epsilon)$ since the kinetic energy release probabilities are weighted by ρ_{vib}. Figure 6 compares the function $A\exp(-10\epsilon)$ with the different experimental and theoretical KERDs. It appears clearly that the shape of the vibrational density of states governs the decreasing part of the prior and modified OTST KERDs, but not that of the experimental one.

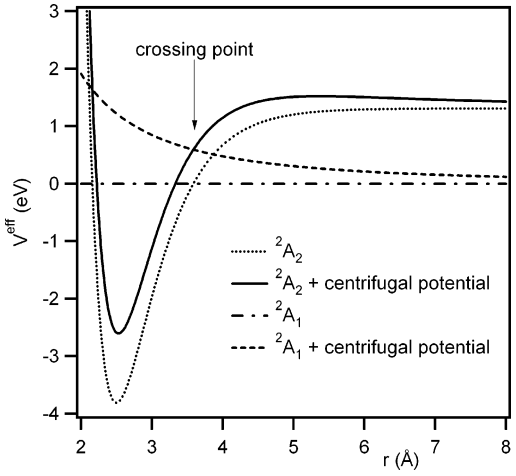

Figure 5. Electronic potential energy curves used in the modified OTST model described in the text (section VI). Dotted line: $^2A_2$ electronic energy curve. Solid line: sum of the $^2A_2$ electronic energy curve and of the centrifugal potential ($l = 60$). Dashed−dotted line: $^2A_1$ electronic energy curve. Dashed line: sum of the $^2A_1$ electronic energy curve and of the centrifugal potential ($l = 60$).

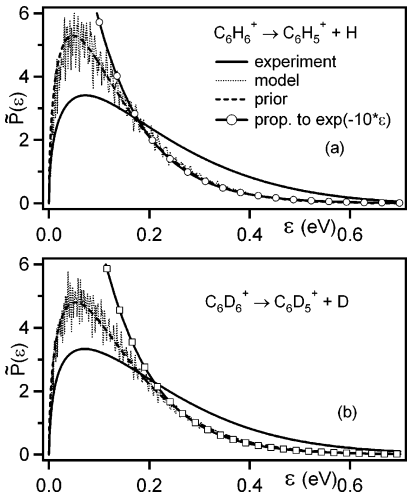

Figure 6. Solid line: experimental KERD for $C_6H_6^+ \rightarrow C_6H_5^+ + H$ (a) and $C_6D_6^+ \rightarrow C_6D_5^+ + D$ (b) for a fragment ion translational energy of 5 keV in the laboratory reference frame. Dashed line: prior KERDs $\tilde{P}^0(\epsilon)$ computed for the same total energy distributions $T(E)$. Dotted line: modified OTST model developed in section VI. Solid line with open symbols: fit of the prior KERD with $A\exp(-10\epsilon)$.

This argument is of qualitative value only. Clearly, however, the larger the number of vibrational degrees of freedom of the phenyl ion that play a role in the dynamics, the larger is ω and the steeper is the decrease of the kinetic energy release distribution. The fact that the actual KERD decreases less rapidly than the prior or than the modified OTST KERDs indicates that dynamical constraints tend to reduce the number of active internal degrees of freedom.

It will be shown in section VII that the statistical adiabatic channel model (SACM) lends itself better than OTST to the

incorporation of the electronically nonadiabatic nature of the reaction.

VII. An Electronically Nonadiabatic Version of SACM

Two dynamical effects are expected to play an essential role for C−H cleavage in $C_6H_6^+$. First, in the study of the dynamics of barrierless unimolecular reactions, it is essential to partition the nuclear degrees of freedom between conserved and transitional modes. The former remain bound during the entire reaction and can be assumed to conserve their vibrational quantum number over the entire reaction path. Transitional modes, on the other hand, consist of the overall rotational degrees of freedom plus the vibrations that eventually convert to a rotation or a translation of the fragments. The second essential aspect, characteristic of the benzene cation, is the already mentioned intrinsic electronically nonadiabatic nature of the H-loss reaction. The purpose of this section is to discuss a model that integrates both aspects.

To study the transformation of transitional modes as the reaction coordinate is stretched, Quack and Troe have proposed that one should define a set of effective potential energy curves.[45−47] In principle, these so-called statistical adiabatic channel (SAC) energy curves should result from an adiabatic separation in which the motion along the reaction coordinate is assumed to be determined by the average potential provided by the fast motion of the other nuclear degrees of freedom.

Although the title of this section may then appear as a contradiction in terms, it is not. In the problem at hand, it is essential to maintain a clear distinction between electronic and vibrotational nonadiabaticity. What is being looked for is a construction of two sets of vibrotationally adiabatic channel energy curves calculated independently for each electronic state. Electronic nonadiabaticity will then operate between compatible pairs of SACM curves (more on this later) associated with each electronic state. In subsections VIIA and VIIB, we discuss the linear model used to describe the electronic nonadiabatic transitions and the reduction of active vibrational space that these transitions imply. How the SACM curves are constructed is then described in subsection VIIC together with a discussion of the proposed reaction mechanism and of its implications.

A. The Linear Model. The rate constant of the dissociation reaction and the cross-section of the reverse capture process are both proportional to the probability of switching from one electronic diabatic state to the other ($^2A_2 \rightarrow {}^2A_1$ or vice versa) (see eq 1.1a). Equivalently, both are proportional to the probability of staying in the lower adiabatic state (i.e., that of staying on the lower sheet of the double cone).

The theory of electronically nonadiabatic transitions is based on the interplay between two possible basis sets of electronic functions. Let us consider a problem restricted to only two electronic states interacting in a multidimensional vibrational subspace spanned by $3N - 6$ vibrational coordinates Q_j, N being the number of atoms in the system. The adiabatic set consists of two eigenfunctions (ψ_1, ψ_2) of the electronic Hamiltonian H. On the other hand, one can also consider the diabatic set (χ_1, χ_2), which arises from the desire to deal with functions whose physical character (ionic, covalent, Rydberg, n−π*, etc.) remains unaltered as the nuclear geometry changes. Diabatic states are required to diagonalize the nuclear momentum matrix:[72−76]

$$\langle \chi_1 | \nabla_{\mathbf{Q}} | \chi_2 \rangle = 0 \tag{7.1}$$

where ∇_Q represents the gradient operator ($\partial/\partial Q_1$,..., $\partial/\partial Q_{3N-6}$).

Two diabatic potential energy surfaces H_{11} and H_{22} and the off-diagonal coupling element H_{12} are then defined by the equation:

$$H_{mn} = \langle \chi_m | H | \chi_n \rangle \quad (m, n = 1, 2) \tag{7.2}$$

The adiabatic potential energy surfaces $U(\mathbf{Q})$ are obtained by diagonalizing the electronic Hamiltonian[73−75]

$$U(\mathbf{Q}) = [H_{11}(\mathbf{Q}) + H_{22}(\mathbf{Q})]/2 \pm \{[H_{22}(\mathbf{Q}) - H_{11}(\mathbf{Q})]^2 + 4H_{12}(\mathbf{Q})^2\}^{1/2} \tag{7.3}$$

A decisive simplification obtains if it is realistic to assume that the diabatic surfaces are planes (in a multidimensional space) that cross along a so-called seam. Consider a particular reference point $\mathbf{Q}_0$ located on the seam and take it as the zero of the energy scale. Then, the series expansion of each matrix element H_{mn} in the diabatic set about point $\mathbf{Q}_0$ can be limited to its first nonzero term:

$$H_{mn}(\mathbf{Q}) = H^{(0)}_{mn}(\mathbf{Q}_0) + \sum_{j=1}^{3N-6} \left\langle \chi_m(\mathbf{Q}_0) \left| \left(\frac{\partial H}{\partial Q_j} \right)_{\mathbf{Q}_0} \right| \chi_n(\mathbf{Q}_0) \right\rangle Q_j = H^{(0)}_{mn}(\mathbf{Q}_0) + \sum_{j=1}^{3N-6} H^{(1)}_{mn,j} Q_j \tag{7.4}$$

where the superscript in parentheses indicates the order of the derivative. A system that fulfils these assumptions is said to obey the linear model.[73−75]

If the nonadiabatic interaction involves two electronic states of different symmetry, as in a conical intersection, then the zero-order off-diagonal matrix element $H^{(0)}_{12,j}$ vanishes. For an avoided crossing, $H^{(0)}_{12,j}$ does not vanish and constitutes the leading term. This circumstance is responsible for a qualitative difference between the two types of interaction.

The two sets (ψ_1, ψ_2) and (χ_1, χ_2) are related by an orthogonal transformation parametrized by an angle $\theta(\mathbf{Q})$.

$$\begin{bmatrix} \psi_1 = \chi_1 \cos\theta(\mathbf{Q}) + \chi_2 \sin\theta(\mathbf{Q}) \\ \psi_2 = -\chi_1 \sin\theta(\mathbf{Q}) + \chi_2 \cos\theta(\mathbf{Q}) \end{bmatrix} \tag{7.5}$$

One has:

$$\tan[2\theta(\mathbf{Q})] = 2H_{12}(\mathbf{Q})/[H_{22}(\mathbf{Q}) - H_{11}(\mathbf{Q})] \tag{7.6}$$

A nonadiabatic transition can be induced by a particular nuclear motion only if the angle $\theta(\mathbf{Q})$ varies along the corresponding classical trajectory.[72−74] It is important to note that only a subspace of the total configuration space determines the transition probability, as shown explicitly in the next section.

B. Dimensionality Reduction. Define three ($3N - 6$) dimensional vectors $\boldsymbol{\xi}_\mathbf{A}$, $\boldsymbol{\xi}_\mathbf{B}$, and $\boldsymbol{\xi}_\mathbf{C}$ whose components involve the matrix elements $H^{(1)}_{mn,j}$ [75]

$$\xi_{Aj} = H^{(1)}_{22,j} + H^{(1)}_{11,j} \tag{7.7a}$$

$$\xi_{Bj} = H^{(1)}_{22,j} - H^{(1)}_{11,j} \tag{7.7b}$$

$$\xi_{Cj} = H^{(1)}_{12,j} \tag{7.7c}$$

Vector $\boldsymbol{\xi}_\mathbf{B}$ is in fact the gradient of the energy gap $H_{22} - H_{11}$ between the two diabatic planes. If the nonadiabatic interaction is the last step of a unimolecular dissociation, $\boldsymbol{\xi}_\mathbf{B}$ is the reaction coordinate. Vector $\boldsymbol{\xi}_\mathbf{C}$ represents the direction along which the coupling matrix element H_{12} increases most rapidly. In principle,

for a conical intersection, ξ_C is a linear combination of symmetry lowering modes.

Inserting eqs 7.7 into eq 7.3,

$$U(\mathbf{Q}) = (1/2)\{\boldsymbol{\xi}_\mathbf{A}\cdot\mathbf{Q} \pm [(\boldsymbol{\xi}_\mathbf{B}\cdot\mathbf{Q})^2 + 4(\boldsymbol{\xi}_\mathbf{C}\cdot\mathbf{Q})^2]^{1/2}\} \quad (7.8)$$

leads to the equation of a double cone with its vertex at the origin. Further substituting eqs 7.7 into eq 7.6, one obtains

$$\tan[2\theta(\mathbf{Q})] = 2\boldsymbol{\xi}_\mathbf{C}\cdot\mathbf{Q}/\boldsymbol{\xi}_\mathbf{B}\cdot\mathbf{Q} \quad (7.9)$$

Hence, for a conical intersection, only the projection of the nuclear trajectory on the two-dimensional subspace spanned by the two vectors $\boldsymbol{\xi}_\mathbf{B}$ and $\boldsymbol{\xi}_\mathbf{C}$ can bring about a variation of the angle $\theta(\mathbf{Q})$ and therefore a nonzero transition probability.

The conclusion can thus be drawn that only a very small subspace of the vibrational configuration space is important for the calculation of the transition probability. This implies that only that part of the vibrational energy that flows into a few particular degrees of freedom determines the reaction dynamics at the conical intersection. The reliability of this conclusion depends of course on the validity of the linear model. In fact, the dimension of the active subspace depends on the order of the terms that have to be retained in a meaningful expansion of the matrix elements $H_{mn}(\mathbf{Q})$. Furthermore, the influence of the rotational degrees of freedom has been so far completely disregarded. Thus, one is not dealing here with a strict selection rule, but rather with a kind of propensity rule.

The next step consists of evaluating how the nonadiabatic transition probability is affected by the inclusion of the transitional degrees of freedom.

C. SACM Energy Curves for the Benzene Dissociation. In practice, the effective SACM potential curves (also termed channel energies) are often obtained by an interpolation between the situation valid at the equilibrium position (i.e., a set of oscillators) and that valid for an infinite separation of the fragments (i.e., a set of rotational, orbital, and translational motions).[45,46] In a barrierless reaction, the reaction dynamics is mainly controlled by the conservation of angular momentum. This constraint concerns essentially the transitional modes.

We now follow a previous attempt to extend SACM to electronically nonadiabatic transitions.[76]

(1) Channel Energy Curves for the $^2A_2$ Diabatic State. These effective potential energy curves are expressed as the sum of three contributions: electronic, vibrotational, and centrifugal.

(i) The electronic contribution is parametrized by the Morse equation (as in Figure 5).

(ii) The second contribution results from an interpolation between a nearly doubly degenerate CH rocking vibration ν_{rock} and the two-dimensional rotation of the phenyl ion fragment characterized by its rotational constant B. The interpolation function $C(r)$ is simply taken as an exponential [45,46]

$$C(r) = \exp[-\alpha(r - r_{eq})] \quad (7.10)$$

where r is the distance between the center of the phenyl ion and the H atom, r_{eq} being the equilibrium value and $\alpha \approx \beta/2$, β being the parameter of the Morse equation.

(iii) The centrifugal energy is defined[45] as $p(p+1)h^2/(2\mu r^2)$ where μ is the reduced mass of the system and p is a "rotational pseudo-quantum number", which, however, depends on the value of the reaction coordinate. It is obtained by interpolation between the overall angular momentum J of the molecular ion at its equilibrium geometry and the orbital angular momentum l generated by the centrifugal motion of the fragments:

$$p(r) = JC(r) + [1 - C(r)]l \quad (7.11)$$

This contribution vanishes asymptotically. The adiabatic potential energy curves of the $^2A_2$ fragment thus obey the following equation:

$$V_2(r,J,n,j,l) = D_2\{1 - \exp[-\beta(r - r_{eq})]\}^2 - D_2 + D_{12} + (n+1)h\nu_{rock}C(r) + [1 - C(r)]B\,j(j+1) + p(p+1)\hbar^2/(2\mu r^2) \quad (7.12)$$

where n is the vibrational quantum number of the degenerate CH rocking vibration, D_2 is the dissociation energy of the $^2A_2$ state and D_{12} is the energy difference between the dissociation asymptotes of the $^2A_2$ and $^2A_1$ states. Note that in the range of internuclear distances where the reaction takes place, the (conserved) total angular momentum $J\hbar$ is partitioned into two components: fragment rotation (quantum number j), and orbital motion [position-dependent pseudo-quantum number $p(r)$].

(2) Channel Energy Curves for the $^2A_1$ Diabatic State. The $^2A_1$ diabatic state is characterized by a nearly flat potential energy curve (which asymptotically defines the zero of the energy scale). Since the forces that derive from this potential are negligible, the two particles are free and their motions are independent. The hydrogen atom travels along a rectilinear trajectory while the phenyl ion undergoes a rotational motion. An impact parameter b can be defined to parametrize the position of the two moieties.

The channel energy curves can be derived from those of the $^2A_2$ potential by letting the parameters of the Morse curve (D_2, D_{12}, β, and hence α) tend to zero. The electronic contribution vanishes and so does the vibrotational component (because the rocking frequency is equal to zero in a flat potential). The equation of the effective potential energy curves thus reads simply

$$V_1(r,J) = J(J+1)\hbar^2/(2\mu r^2) \quad (7.13)$$

Note in addition that even if the potential is absolutely flat, i.e., in the absence of any force, the linear motion of the hydrogen atom is characterized by an angular momentum equal to $b(2\mu\epsilon)^{1/2}$. A second component to the angular momentum in the $^2A_1$ state comes from the rotational motion of the phenyl ion fragment.

(3) The Electronically Nonadiabatic Transition. At the crossing point between two potential energy curves obeying the compatibility condition defined below, a nonadiabatic transition is possible, during which a strongly coupled system (in the $^2A_2$ state) suddenly decouples as it converts to the $^2A_1$ state. To determine the compatibility, it can be assumed that the rotational quantum number j of the heavy phenyl ion remains conserved during the nonadiabatic transition. It then follows quite naturally that the second component of the angular momentum, which results from the motion of the light hydrogen atom and which is equal to $b(2\mu\epsilon)^{1/2}$ in the $^2A_1$ state, converts into that deriving from the pseudo-quantum number p evaluated at the crossing point r_c:

$$b\sqrt{2\mu\epsilon} = \hbar p(r_c) = J\hbar C(r_c) + [1 - C(r_c)]l\hbar \quad (7.14)$$

Effective potential energy curves in the $^2A_2$ state were generated for various quantum numbers n, j, l and J. The pseudo-quantum number p was then calculated at the point where these curves

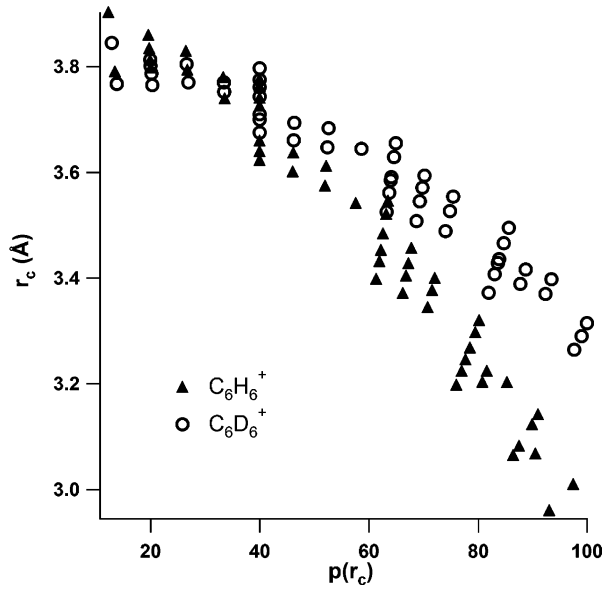

Figure 7. Curve crossing positions, r_c, as a function of the pseudo-quantum number, p, defined by eq 7.11. Full triangles: $C_6H_6^+ \rightarrow C_6H_5^+ + H$. Open circles: $C_6D_6^+ \rightarrow C_6D_5^+ + D$. The displayed data correspond to a representative sampling of (J,l,j) combinations. Despite the data point dispersion, a decrease of r_c for increasing p clearly emerges, especially for the undeuterated species.

crossed the line $J(J+1)h^2/(2\mu r^2)$. A strong correlation emerged from these calculations (Figure 7): a large value of l or p results in a low value of r_c. This result is of importance because the lower r_c, the larger the value of the off-diagonal matrix element of the electronic Hamiltonian $H_{12}(r_c)$ between the two diabatic functions and therefore the higher the transition probability. This can be seen as follows.

For a conical intersection, the nonadiabatic transition probability can be expressed by an equation that is very similar to the Landau−Zener formula:[73−75]

$$P = \exp\left(-\frac{2\pi {H_{12}}^2}{\hbar v \Delta F}\right) \qquad (7.15)$$

The values of the three quantities H_{12}, v, and ΔF that appear in this equation depend on r_c, the crossing point between the diabatic curves. However, the off-diagonal element H_{12} is expected to vary extremely rapidly with r_c,[76] in contradistinction to v and ΔF.

Furthermore, similar calculations have been carried out for the fragmentation of the perdeuterated species (reaction 1.1b). The correlation between l and r_c is still present but appears to be less significant because the slope of the $r_c(l)$ curve is smaller (Figure 7). This result agrees with our experimental observation that, at a given energy E, the translational energy release is lower for reaction 1.1b than for reaction 1.1a (Figure 3) and is closer to the statistical expectation for the perdeuterated ion. This is an additional argument in favor of the present model.

VIII. Summary and Concluding Remarks

The C−H cleavage reaction in the benzene cation is observed to release more translational kinetic energy on the fragments than expected on statistical grounds. We suggest relating this observation to the intrinsically nonadiabatic nature of this reaction pathway. At the internal energies sampled in our experiments, only the lowest dissociation asymptote can be reached, i.e., $C_6H_5^+(^1A_1) + H(^2S)$. This requires a nonadiabatic transition involving a conical intersection between the strongly attractive $^2A_2$ state and the basically flat $^2A_1$ state that leads to ground-state fragments. This transition is associated with a reduction of the dimensionality of the active vibrational configuration space, thus decreasing the density of active vibrational states and increasing the average translational energy released.

The curve-crossing mechanism that has been proposed predicts an increase of the dissociation rate constant of the attractive $^2A_2$ state as the final orbital angular momentum increases, i.e., as the relative kinetic energy of the fragments increases. Three mechanisms seem to operate in this nonadiabatic transition.

The higher the quantum numbers of the transitional modes [n, j, l, $p(r_c)$], the shorter the value of r_c at which the channel energies cross. Hence, the higher the energy that flows into these degrees of freedom, the larger the probability of undergoing the electronic nonadiabatic transition between the $^2A_2$ and $^2A_1$ states.

As described in section V, the transition from the $^2A_2$ to the $^2A_1$ state must be accompanied by a structural rearrangement of the phenyl moiety. As a consequence, the higher the vibrational energy deposited in the conserved modes specifically associated with the deformation of the aromatic cycle, the higher the probability of readjusting its geometry.

In the SACM model, just as in OTST, a high value of the orbital quantum number l may generate a large centrifugal barrier that may block the reaction channel (i.e., make it unable to participate in the kinetics). However, this is seldom the case in practice in our model because the crossing point r_c between effective channel energy curves takes place at values of the reaction coordinate much shorter than the position of the top of the centrifugal barrier: the ion abandons the $^2A_2$ state and switches to the flat $^2A_1$ potential before being influenced by the barrier.

Once the $^2A_2$ to $^2A_1$ transition has been performed, the system remains on the flat $^2A_1$ potential energy surface. Long-range forces are no longer present between the receding fragments that can be considered as separated. Vibrational or rotational nonadiabaticity which would take place after crossing the conical intersection can thus be excluded in the particular reaction studied here.

The present work was only concerned with the specific case of the $C_6H_6^+$ ion. It seems, however, to be a common characteristic of H-loss reactions that they release more translational energy than the statistical estimate.[26−30] Clearly, very few of them are electronically nonadiabatic. Alternative mechanisms must therefore operate. In a study of the benzylium ion formation from the toluene cation,[30] it has been argued that rotational energy flows preferentially into the reaction coordinate. Rovibrational nonadiabaticity can also be expected to play a role, especially for H loss reactions where the motion along the reaction coordinate becomes fast compared to the rotational motion. As suggested by the work of Mardis and Sibert,[78] the transition probability between rotational channels tends to increase with increasing relative translational energy. Although not explicitly mentioned by these authors, this mechanism could give rise to an interesting phenomenon. Transitions to lower rotational channels are accompanied by an increase of the relative translational energy which would in turn increase the probability of further transitions and so on. The building of such a constructive loop might provide a plausible mechanism for electronically adiabatic hydrogen loss reactions.

Acknowledgment. This paper is dedicated to the memory of Chava Lifshitz, in recognition of her many contributions to

the fundamental aspects of ion chemistry. Financial support from the Belgian FNRS (Crédit aux chercheurs to B.L.) and from the Gouvernement de la Communauté Française de Belgique, via an "Action de Recherche Concertée" (ARC 99-04/245), is gratefully acknowledged.

References and Notes

(1) Andlauer, B.; Ottinger, C. *J. Chem. Phys.* **1971**, *55*, 1471.
(2) Rosenstock, H. M.; Larkins, J. T.; Walker, J. A. *Int. J. Mass Spectrom. Ion Phys.* **1973**, *11*, 309.
(3) Chupka, W. A. In *Chemical Spectroscopy and Photochemistry in the Vacuum-Ultraviolet*; Sandorfy, C., Ausloos, P. J., Robin, M. B., Eds.; Reidel: Dordrecht, The Netherlands, 1974.
(4) Eland, J. H. D.; Schulte, H. *J. Chem. Phys.* **1975**, *62*, 3835.
(5) Eland, J. H. D.; Frey, R.; Schulte, H.; Brehm, B. *Int. J. Mass Spectrom. Ion Phys.* **1976**, *21*, 209.
(6) Rosenstock, H. M.; McCulloh, K. E.; Lossing, F. P. *Int. J. Mass Spectrom. Ion Phys.* **1977**, *25*, 327.
(7) Baer, T.; Willett, G. D.; Smith, D.; Phillips, J. S. *J. Chem. Phys.* **1979**, *70*, 4076.
(8) Jarrold, M. F.; Wagner-Redeker, W.; Illies, A. J.; Kirchner, N. J.; Bowers, M. T. *Int. J. Mass Spectrom. Ion Processes* **1984**, *58*, 63.
(9) Kühlewind, H.; Neusser, H. J.; Schlag, E. W. *J. Phys. Chem.* **1984**, *88*, 6104.
(10) Neusser, H. J.; Kühlewind, H.; Boesl, U.; Schlag, E. W. *Ber. Bunsen Ges. Phys. Chem.* **1985**, *89*, 276.
(11) Kühlewind, H.; Kiermeier, A.; Neusser, H. J. *J. Chem. Phys.* **1986**, *85*, 4427.
(12) Kühlewind, H.; Kiermeier, A.; Neusser, H. J.; Schlag, E. W. *J. Chem. Phys.* **1987**, *87*, 6488.
(13) Kiermeier, A.; Kühlewind, H.; Neusser, H. J.; Schlag, E. W.; Lin, S. H. *J. Chem. Phys.* **1988**, *88*, 6182.
(14) Neusser, H. J. *J. Phys. Chem.* **1989**, *93*, 3897.
(15) Grebner, T. L.; Neusser, H. J. *Int. J. Mass Spectrom.* **1999**, *185/186/187*, 517.
(16) Klippenstein, S. J.; Faulk, J. D.; Dunbar, R. C. *J. Chem. Phys.* **1993**, *98*, 243.
(17) Holland, D. M. P.; Shaw, D. A.; Sumner, I.; Bowler, M. A.; Mackie, R. A.; Shpinkova, L. G.; Cooper, L.; Rennie, E. E.; Parker, J. E.; Johnson, C. A. F. *Int. J. Mass Spectrom.* **2002**, *220*, 31.
(18) Klots, C. E. *J. Chem. Phys.* **1990**, *93*, 2513.
(19) Klots, C. E. *J. Chem. Phys.* **1990**, *93*, 6585.
(20) Klippenstein, S. J. *Int. J. Mass Spectrom. Ion Processes* **1997**, *167/168*, 235.
(21) Klots, C. E. *J. Chem. Phys.* **1976**, *64*, 4269.
(22) Bertrand, M.; Beynon, J. H.; Cooks, R. G. *Int. J. Mass Spectrom. Ion Phys.* **1972**, *9*, 346.
(23) Jones, E. G.; Bauman, L. E.; Beynon, J. H.; Cooks, R. G. *Org. Mass Spectrom.* **1973**, *7*, 185.
(24) Cooks, R. G.; Kim, K. C.; Keough, T.; Beynon, J. H. *Int. J. Mass Spectrom. Ion Phys.* **1974**, *15*, 271.
(25) Migahed, M. D.; Abd El-Kader, F. H. *Int. J. Mass Spectrom. Ion Phys.* **1978**, *28*, 225.
(26) Lifshitz, C. *Int. J. Mass Spectrom. Ion Processes* **1992**, *118*−*119*, 315.
(27) Park, J.; Bersohn, R.; Oref, I. *J. Chem. Phys.* **1990**, *93*, 5700.
(28) Chesnavich, W. J.; Bass, L.; Su, T.; Bowers, M. T. *J. Chem. Phys.* **1981**, *74*, 2228.
(29) Blank, D. A.; Suits, A. G.; Lee, Y. T.; North, S. W.; Hall, G. E. *J. Chem. Phys.* **1998**, *108*, 5784.
(30) Fati, D.; Lorquet, A. J.; Locht, R.; Lorquet, J. C.; Leyh, B. *J. Phys. Chem. A* **2004**, *108*, 9777.
(31) Gridelet, E.; Lorquet, J. C.; Leyh, B. *J. Chem. Phys.* **2005**, *122*, 094106.
(32) Chesnavich, W. J.; Bowers, M. T. *J. Chem. Phys.* **1977**, *66*, 2306.
(33) Chesnavich, W. J.; Bowers, M. T. *J. Am. Chem. Soc.* **1977**, *99*, 1705.
(34) Chesnavich, W. J.; Bowers, M. T. *Prog. React. Kinet.* **1982**, *11*, 137.
(35) Baer, T.; Hase, W. L. *Unimolecular Reaction Dynamics. Theory and Experiments*; Oxford University: New York, 1996.
(36) Laskin, J.; Lifshitz, C. *J. Mass Spectrom.* **2001**, *36*, 459.
(37) Leyh, B.; Lorquet, J. C. Kinetic energy release distributions in mass spectrometry. In *The Encyclopedia of Mass Spectrometry*; Armentrout, P. B., Ed.; Elsevier: Amsterdam, 2003; Vol. 1; p 17.
(38) Nicolaides, A.; Smith, D. M.; Jensen, F.; Radom, L. *J. Am. Chem. Soc.* **1997**, *119*, 8083.
(39) Harvey, J. N.; Aschi, M.; Schwarz, H.; Koch, W. *Theor. Chem. Acc.* **1998**, *99*, *95*.
(40) Levine, R. D.; Kinsey, J. L. In *Atom-Molecule Collision Theory. A Guide for the Experimentalist*; Bernstein, R. B., Ed.; Plenum: New York, 1979.
(41) Levine, R. D. *Adv. Chem. Phys.* **1981**, *47*, 239.
(42) Levine, R. D.; Bernstein, R. B. In *Dynamics of Molecular Collisions, Part B*; Miller, W. H., Ed.; Plenum: New York, 1976.
(43) Urbain, P.; Remacle, F.; Leyh, B.; Lorquet, J. C. *J. Phys. Chem.* **1996**, *100*, 8003.
(44) Urbain, P.; Leyh, B.; Remacle, F.; Lorquet, A. J.; Flammang, R.; Lorquet, J. C. *J. Chem. Phys.* **1999**, *110*, 2911.
(45) Quack, M.; Troe, J. *Ber. Bunsen Ges. Phys. Chem.* **1974**, *78*, 240.
(46) Quack, M.; Troe, J. *Ber. Bunsen Ges. Phys. Chem.* **1975**, *79*, 469.
(47) Lorquet, J. C.; Leyh, B. Statistical theories in mass spectrometry. In *The Encyclopedia of Mass Spectrometry*; Armentrout, P. B., Ed.; Elsevier: Amsterdam, 2003; Vol. 1; p 8.
(48) Barber, M.; Elliot, R. M. 12th Annual Conference on Mass Spectrometry, Montreal, Canada, ASTM E−14, 1964.
(49) Jennings, K. R. *J. Chem. Phys.* **1965**, *43*, 4176.
(50) Barber, M.; Green, B. N.; Wolstenholme, W. A.; Jennings, K. R. *Adv. Mass Spectrom.* **1968**, *4*, 89.
(51) Beynon, J. H.; Fontaine, A. E.; Lester, G. R. *Int. J. Mass Spectrom. Ion Phys.* **1972**, *8*, 341.
(52) Cooks, R. G.; Beynon, J. H.; Caprioli, R. M.; Lester, G. R. *Metastable Ions*; Elsevier: Amsterdam, 1973.
(53) Holmes, J. L.; Osborne, A. D. *Int. J. Mass Spectrom. Ion Phys.* **1977**, *23*, 189.
(54) Szilagyi, Z.; Vekey, K. Eur. *Mass Spectrom.* **1995**, *1*, 507.
(55) Rumpf, B. A.; Derrick, P. J. *Int. J. Mass Spectrom. Ion Processes* **1988**, *82*, 239.
(56) Yeh, I. C.; Kim, M. S. *Rapid Commun. Mass Spectrom.* **1992**, *6*, 115.
(57) Lias, S. G.; Bartmess, J. E.; Liebman, J. F.; Holmes, J. L.; Levin, R. D.; Mallard, W. G. *Gas-Phase Ion* and Neutral Thermochemistry, *J. Phys. Chem. Ref. Data* **1988**, *17*.
(58) Levine, R. D.; Bernstein, R. B. *Molecular Reaction Dynamics and Chemical Reactivity*; Oxford University: New York, 1987.
(59) Levine, R. D. *Molecular Reaction Dynamics*; Cambridge University Press: Cambridge, U.K., 2005.
(60) Alhassid, Y.; Levine, R. D. *J. Chem. Phys.* **1977**, *67*, 4321.
(61) Urbain, P.; Leyh, B.; Remacle, F.; Lorquet, J. C. *Int. J. Mass Spectrom.* **1999**, *185/186/187*, 155.
(62) Hoxha, A.; Locht, R.; Lorquet, A. J.; Lorquet, J. C.; Leyh, B. *J. Chem. Phys.* **1999**, *111*, 9259.
(63) Gridelet, E.; Locht, R.; Lorquet, A. J.; Lorquet, J. C.; Leyh, B. *Int. J. Mass Spectrom.* **2003**, *228*, 389.
(64) Gridelet, E.; Dehareng, D.; Locht, R.; Lorquet, A. J.; Lorquet, J. C.; Leyh, B. *J. Phys. Chem. A* **2005**, *109*, 8225.
(65) Iachello, F.; Levine, R. D. *Europhysics Lett.* **1987**, *4*, 389.
(66) Moon, J. H.; Choe, J. C.; Kim, M. S. *J. Phys. Chem. A* **2000**, *104*, 458.
(67) Locht, R. *Int. J. Mass Spectrom. Ion Processes* **1995**, *148*, L17.
(68) Servais, C.; Locht, R. *Chem. Phys. Lett.* **1995**, *236*, 96.
(69) Zamir, E.; Levine, R. D. *Chem. Phys.* **1980**, *52*, 253.
(70) Delos, J. B. *J. Chem. Phys.* **1973**, *59*, 2365.
(71) Bandrauk, A. D.; Laplante, J. P. *J. Chem. Phys.* **1976**, *65*, 2592.
(72) Desouter-Lecomte, M.; Lorquet, J. C. *J. Chem. Phys.* **1979**, *71*, 4391.
(73) Nikitin, E. E.. *Theory of Elementary Atomic and Molecular Processes in Gases;* Clarendon Press: Oxford, U.K., 1974.
(74) Desouter-Lecomte, M.; Dehareng, D.; Leyh-Nihant, B.; Praet, M. T.; Lorquet, A. J.; Lorquet, J. C. *J. Phys. Chem.* **1985**, *89*, 214.
(75) Desouter-Lecomte, M.; Leyh-Nihant, B.; Praet, M. T.; Lorquet, J. C. *J. Chem. Phys.* **1987**, *86*, 7025.
(76) Leyh-Nihant, B.; Lorquet, J. C. *J. Chem. Phys.* **1988**, *88*, 5606.
(77) Lorquet, J. C.; Leyh, B. Nonadiabatic Reactions. In *The Encyclopedia of Mass Spectrometry*; Armentrout, P. B., Ed.; Elsevier: Amsterdam, 2003; Vol. 1; p 33.
(78) Mardis, K. L.; Sibert, E. L., III. *J. Chem. Phys.* **1998**, *109*, 8897.